Bridge State and Average Train Axle Mass Estimation for Adaptive Railway Bridges

Amelie Zeller, Spasena Dakova, Charlotte Stein, Michael Böhm, Gennaro Senatore, Arka P. Reksowardojo, Lucio Blandini, Oliver Sawodny, *Senior Member, IEEE*, and Cristina Tarín

***Abstract*—Adaptive structures are equipped with sensors and actuators to counteract deformations caused by external loads. Concerning railway bridges, previous work has shown that active vibration damping allows to extend the service life. Trains as external loads represent the decisive influencing factor for bridge vibration and has to be taken into account when applying model-based control concepts. This article proposes a state and disturbance estimator (SDE) for bridge structures based on a moving point load train model and estimating the average train axle mass. The model employed for state and disturbance estimation is linear time variant, which allows use of an augmented Kalman filter. Estimability is analyzed based on the Fisher information and the proposed state and disturbance estimator (SDE) is systematically tested through simulations. A linear quadratic regulator is designed and combined with the proposed SDE to evaluate the closed-loop performance for damping the bridge vibrations during train crossing.**

***Index Terms*—Adaptive structures, application, disturbance estimation, mechatronic systems, railway bridges, state estimation.**

I. Introduction

THE construction sector is the largest single contributor to greenhouse gas emissions and resource consumption worldwide. To mitigate adverse effects of climate change and to meet the demand for buildings and infrastructure due to the growing world population, there is a need to build more with fewer resources and/ or to extend the service life of existing structures.

Manuscript received 15 January 2023; revised 30 March 2023; accepted 9 May 2023. Date of publication 7 June 2023; date of current version 16 August 2023. Recommended by Technical Editor Y. Li and Senior Editor Q. Zou. This work was supported by the Deutsche Forschungsgemeinschaft (DFG, German Research Foundation) under Grant 279064222 and Grant SFB1244, collaborative research center 1244 (CRC1244). Subproject B02 in collaboration with C07 and B04. *(Corresponding author: Amelie Zeller.)*

The authors are with the Institute for System Dynamics, Institute for Lightweight Structures, and Conceptual Design, University of Stuttgart, 70563 Stuttgart, Germany (e-mail: amelie.zeller@isys.uni-stuttgart.de; spasena.dakova@isys.uni-stuttgart.de; charlotte.stein@isys.uni-stuttgart.de; michael.boehm@isys.uni-stuttgart.de; gennaro.senatore@ilek.uni-stuttgart.de; arka.reksowardojo@ilek.uni-stuttgart.de; lucio.blandini@ilek.uni-stuttgart.de; oliver.sawodny@isys.uni-stuttgart.de; cristina.tarin-sauer@isys.uni-stuttgart.de).

Color versions of one or more figures in this article are available at https://doi.org/10.1109/TMECH.2023.3277317.

Digital Object Identifier 10.1109/TMECH.2023.3277317

Adaptive structures are equipped with sensors and actuators to compensate for displacements and vibrations caused by external loads. Previous work has shown that this can provide significant savings in resources, emissions, and service life [1], [2], [3]. For railway bridges, vibration during train passage is the main cause of deterioration and many railroad bridges built in Europe are nearing the end of their service life [4]. This motivates research into new adaptive bridges, adaptive retrofit systems for existing bridges and control concepts for vibration control to extend service life.

In general, external loads are the decisive influencing factors for displacements and vibrations of structures, e.g., wind loads for high-rises or trains for railway bridges. Considering railway bridges, the forces between the train wheels and the contact points at the bridge cause a downward displacement of the bridge and since the contact points move along the bridge, periodic forces act at the bridge causing vibrations. These forces represent the load for the bridge, referred to by disturbance in the following. In general, to compensate displacements or damp vibrations of structures, by employing their adaptive system and control algorithms, the disturbances have to be taken into account. These loads can either be measured or, as we propose in this work for a railway bridge, reconstructed using an state and disturbance estimator (SDE).

The frequencies of the periodic disturbances can be calculated as the quotient of the train speed and the wheelbases. If they coincide with any of the bridge's eigenfrequencies or their higher harmonics, high vibration amplitudes can occur, called vehicle-driven resonances. This article deals with a short bridge, for which slow trains usually only excite the second and higher harmonics. High-speed trains can excite the first harmonics causing higher vibration amplitudes [3] and are thus the most critical load case. However, the proposed SDE is applicable to both slow and high-speed trains.

The bridge considered in this work is equipped with an adaptive external posttensioning system, which has already been investigated in [3] and shows good potential for vibration damping. The bridge structure is modeled by finite element (FE) discretization with beam elements and the bridge state includes displacements, rotations, and velocities of all bridge nodes. The train is modeled by mass-spring-damper systems, one for each train axle, moving along the bridge. Thus, the train axles can oscillate and each contact force includes the weight of the train axle and the spring and damper forces, which depend on the

relative vertical displacement and velocity of the bridge and the train axle mass.

In general, disturbance estimation can be considered in different frameworks, e.g., recursive system identification, online parameter estimation, extended state observation or unknown input observation, and there are many different approaches. Commonly used methods are Kalman filtering or recursive least squares algorithms [5], [6]. In the following, we review literature on SDE for bridges. Instead of the different names used in the literature, we refer to all proposed methods as SDE. Lourens et al. [7] proposed an SDE, whereby the disturbance is modeled by equivalent forces with fixed contact points. The SDE was applied to a pedestrian bridge. Although similar to the configuration considered herein, the disturbance dynamics are different, as the loads acting on a railway bridge change faster than the loads acting on a pedestrian bridge. This SDE was extended in [8] to account for modeling uncertainties and was tested under impulse, harmonic, and swept sine loads at fixed contact points, which are not representative of typical real-world loading scenarios. In [9], an augmented Kalman filter (AKF) was proposed for SDE, which has also been adopted in this work. Experimental testing was carried out on a 3-m long steel beam equipped with accelerometers (at 19 to 34 locations) and under varying loads at fixed contact points. In this work, however, only displacement outputs at three locations will be used and the loads move along the structure. For strain monitoring of steel railway bridges, Azam et al. [10] designed an SDE using an AKF along with sparse strain output. Moving point loads projected onto the vibration modes are employed as a disturbance model. The projections are treated as unknowns to be estimated. In contrast, the algorithm proposed herein estimates the average amplitude of the moving point loads directly. Azam et al. [11] proposed a method for estimating the amplitude of moving point loads based on dynamic programming, which is typically computationally expensive. This method was applied to a beam under two moving point loads with a speed of 40 ms^{-1}. Herein, multiple moving point loads with speeds of up to 80 ms^{-1} are considered.

Little attention has been given to the systematic derivation of a disturbance model suitable for model-based SDE for railway bridges. Preliminary work has been done by Zeller et al. [12], in which state estimation for a bridge is studied assuming no or all information about the disturbance available. As expected, the estimates are significantly better when the full information about the disturbance is available. Then, the bridge state is estimated with the mass-spring-damper train model added to the estimation model. The use of this accurate disturbance model leads to unsatisfactory estimation performance. To improve observability, the disturbance model is reduced to the essentials, here the train axle weight forces, while the train vibrations are subordinate. This reduced disturbance model is referred to as the moving point load (MPL) model, this is sufficient and allows for good state estimation results, as illustrated in [12]. Building upon [12], the main contributions of this work are as follows.

1) The development of an SDE based on an MPL model. Given the train speed and wheelbases, the average train axle mass is estimated in addition to the bridge state. The simplicity of the reduced disturbance model causes the estimation model to be linear time variant (LTV) allowing the use of an AKF.
2) The analysis of the estimability of the average train axle mass using the Fisher information (FI).
3) The evaluation of the algorithm's performance for different train parameters in a simulation study.
4) The evaluation of the closed-loop performance using a linear quadratic regulator (LQR) for vibration damping relying on the estimated bridge state and average train axle mass.

The rest of this article is organized as follows. Section II describes the modeling of the adaptive bridge, the train, and their interaction. Section III compares disturbance models of different complexity for bridge state estimation. Section IV introduces the SDE, followed by an estimability analysis and a simulation study. The effectiveness of the SDE in a closed-loop using an LQR for vibration damping is demonstrated in Section V. Finally, Section VI concludes this article.

II. System Dynamics

The configuration considered in this work is illustrated in Fig. 1. The structure is a simply supported beam bridge with a span of $40\mathrm{m}$. The bridge is equipped with an adaptive external posttensioning system comprising under-deck cables deviated by vertical struts. Linear actuators can change the length of the vertical struts and thus modify the tension in the cables resulting in a bending moment that can be employed to dampen vibrations as the train crosses. The train is modeled by mass-spring-damper systems moving along the bridge. The model comprises the bridge and train dynamics and a coupling term.

A. Bridge Model

The bridge model is adopted from [3]. The structure is discretized by an FE-model made of beam elements. It is planar (in the x-y-plane) comprising 12 nodes and 15 beam elements. Each node has three DOFs: x-displacement (horizontal), y-displacement (vertical), and z-rotation (in-plane). The bridge is supported at the ends, the horizontal and vertical displacements of the leftmost node and the vertical displacement of the rightmost node are constrained. The remaining $n = 33$ DoFs are collected in the degrees of freedom (DOFs) vector $\boldsymbol{q}_{\mathrm{B}}(t) \in \mathbb{R}^n$. For simplicity of notation, the time dependency and the initial conditions are omitted in the following. In addition, the following assumptions hold.

1) Linear elastic material for the bridge, which is justified because only small deformations occur.
2) Prestress in the under-deck cables such that no slack occurs.
3) The simulation output can only contain displacements of the bridge nodes of the FE model; under this condition, for maximum observability, the simulation output comprises the displacements of the nodes marked yellow in Fig. 1.
4) Discrete simulation output with sampling time $\Delta t = 0.001\mathrm{s}$ and additive uncorrelated Gaussian zero-mean output noise $\boldsymbol{w}_k$ with variance $\sigma_{\mathrm{w}}^2 = 10^{-5}$.

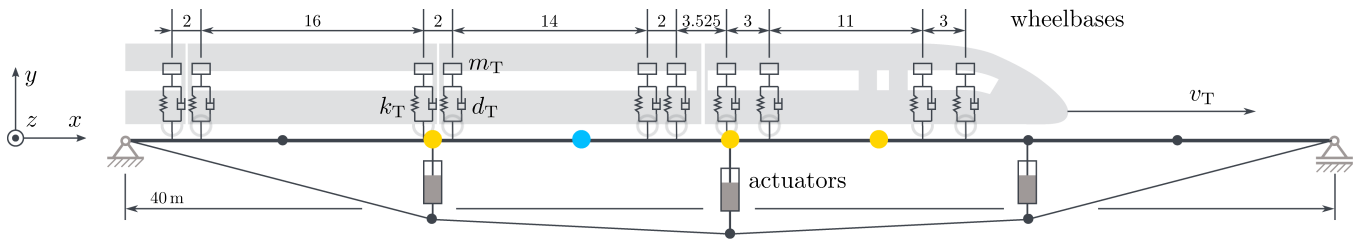

Fig. 1. Bridge-train model. The train axles are represented by mass-spring-damper elements. The external posttensioning system comprises a cable deviated by actuators. All dimensions are in meters.

The equations of motion for the bridge are

$$\boldsymbol{M}_{\mathrm{B}}\ddot{\boldsymbol{q}}_{\mathrm{B}} + \boldsymbol{D}_{\mathrm{B}}\dot{\boldsymbol{q}}_{\mathrm{B}} + \boldsymbol{K}_{\mathrm{B}}\boldsymbol{q}_{\mathrm{B}} = \boldsymbol{z}_{\mathrm{B}} + \boldsymbol{u}_{\mathrm{B}}, \tag{1a}$$

$$\boldsymbol{q}_{\mathrm{B}}(0) = \boldsymbol{q}_{\mathrm{B},0},\ \dot{\boldsymbol{q}}_{\mathrm{B}}(0) = \boldsymbol{q}_{\mathrm{B},1}, t > 0, \tag{1b}$$

where $\dot{\boldsymbol{q}}_{\mathrm{B}}$ and $\ddot{\boldsymbol{q}}_{\mathrm{B}}$ are nodal velocities and accelerations and $\boldsymbol{M}_{\mathrm{B}}, \boldsymbol{K}_{\mathrm{B}} \in \mathbb{R}^{n\times n}$ are positive definite mass and stiffness matrices, respectively. $\boldsymbol{D}_{\mathrm{B}} = \alpha_1\boldsymbol{M}_{\mathrm{B}} + \alpha_2\boldsymbol{K}_{\mathrm{B}}$ is the Rayleigh-damping matrix with $\alpha_1 = 0.05, \alpha_2 = 0.005$ [13].

The disturbance, i.e., the forces acting on the bridge during the train crossing, are collected in $\boldsymbol{z}_{\mathrm{B}} \in \mathbb{R}^n$.

The actuator inputs are denoted by $\boldsymbol{u}_{\mathrm{B}} \in \mathbb{R}^n$. The actuator forces are applied in series with the hosting element as illustrated in Fig. 1. The actuator input can be modeled via forces or displacements. However, the former requires a change in the stiffness matrix, and thus the latter is preferred [14]

$$\boldsymbol{u}_{\mathrm{B}} = \tilde{\boldsymbol{F}}_{\mathrm{B}}\boldsymbol{K}_{\mathrm{el}}\boldsymbol{v}_{\mathrm{B}} = \boldsymbol{F}_{\mathrm{B}}\boldsymbol{v}_{\mathrm{B}} \tag{2}$$

where $\boldsymbol{v}_{\mathrm{B}} \in \mathbb{R}^m$, $m = 3$ contains the actuator displacements, $\boldsymbol{K}_{\mathrm{el}} \in \mathbb{R}^{m\times m}$ is a diagonal matrix containing the stiffness of the actuated elements,and $\tilde{\boldsymbol{F}}_{\mathrm{B}} \in \mathbb{R}^{n\times m}$ maps the resulting actuator forces to the DOFs. Multiplying $\boldsymbol{K}_{\mathrm{el}}$ and $\tilde{\boldsymbol{F}}_{\mathrm{B}}$ forms the input matrix $\boldsymbol{F}_{\mathrm{B}} \in \mathbb{R}^{n\times m}$.

The simulation output is

$$\boldsymbol{y}_k = \boldsymbol{y}(k\Delta t) = \boldsymbol{C}_{\mathrm{B}}\boldsymbol{q}_{\mathrm{B}}(k\Delta t) + \boldsymbol{w}_k,\ k = 1, 2, \ldots \tag{3}$$

where the output matrix $\boldsymbol{C}_{\mathrm{B}} \in \mathbb{R}^{p\times n}$ selects the corresponding displacements from $\boldsymbol{q}_{\mathrm{B}}$ and $p = 6$.

The bridge eigenfrequencies reach up to 1700 Hz. Since the response under train loading is dominated by low-frequency modes, modal reduction is employed. Solving the generalized eigenvalue problem of the undamped model, $(\boldsymbol{K}_{\mathrm{B}} - \omega_{\mathrm{B},i}\boldsymbol{M}_{\mathrm{B}})\boldsymbol{\varphi}_{\mathrm{B},i} = \boldsymbol{0},\ i \in \{1, 2, \ldots, n\}$, gives the eigenfrequencies $\omega_{\mathrm{B},i}$ and the eigenmodes $\boldsymbol{\Phi}_{\mathrm{B}} = [\boldsymbol{\varphi}_{\mathrm{B},1}, \ldots, \boldsymbol{\varphi}_{\mathrm{B},n}]$. The eigenmodes are scaled such that $\boldsymbol{\Phi}_{\mathrm{B}}^{\top}\boldsymbol{M}_{\mathrm{B}}\boldsymbol{\Phi}_{\mathrm{B}} = \boldsymbol{I}$. To obtain a reduced order model, the bridge DOFs are approximated by $\boldsymbol{q}_{\mathrm{B}} = \boldsymbol{\Phi}_{\mathrm{B},r}\boldsymbol{\eta}_{\mathrm{B},r}$, the modal transformation matrix $\boldsymbol{\Phi}_{\mathrm{B},r}$ containing the first r eigenmodes. Inserting this into (1) and (3) and left-multiplying (1) by $\boldsymbol{\Phi}_{\mathrm{B},r}^{\top}$ yields the reduced order model

$$\ddot{\boldsymbol{\eta}}_{\mathrm{B},r} + \boldsymbol{D}_{\mathrm{B},r}\dot{\boldsymbol{\eta}}_{\mathrm{B},r} + \boldsymbol{K}_{\mathrm{B},r}\boldsymbol{\eta}_{\mathrm{B},r} = \boldsymbol{\Phi}_{\mathrm{B},r}^{\top}\boldsymbol{z}_{\mathrm{B}} + \boldsymbol{F}_{\mathrm{B},r}\boldsymbol{v}_{\mathrm{B}} \tag{4a}$$

$$\boldsymbol{y}_k = \boldsymbol{C}_{\mathrm{B},r}\boldsymbol{\eta}_{\mathrm{B},r}(k\Delta t) + \boldsymbol{w}_k, \text{ with} \tag{4b}$$

$$\boldsymbol{D}_{\mathrm{B},r} = \operatorname{diag}(\zeta_{\mathrm{B},i}),\ \zeta_{\mathrm{B},i} = \frac{\alpha_1}{2\omega_{\mathrm{B},i}} + 2\alpha_2\omega_{\mathrm{B},i}$$

$$\boldsymbol{K}_{\mathrm{B},r} = \operatorname{diag}(\omega_{\mathrm{B},i}),\ i \in \{1, \ldots, r\}$$

$$\boldsymbol{F}_{\mathrm{B},r} = \boldsymbol{\Phi}_{\mathrm{B},r}^{\top}\boldsymbol{F}_{\mathrm{B}},\ \boldsymbol{C}_{\mathrm{B},r} = \boldsymbol{C}_{\mathrm{B}}\boldsymbol{\Phi}_{\mathrm{B},r}.$$

In this work $r = 10$ is selected, such that $\omega_{\mathrm{B},r} = 2\pi \cdot 86.5$ Hz.

B. Train Model

The following train model is based on the following three assumptions.

1) Constant train speed v_{T}, since the time span of the train crossing is short, making strong speed changes unlikely.
2) Train speed v_{T} and the points in time at which the train axles enter the bridge $\boldsymbol{t}_{\mathrm{T,x0}}$ are known, since this information is readily available (e.g., measurable by photoelectric sensors).
3) All train axles have individual masses $m_{\mathrm{T},k}$, $k = 1, \ldots, q$, but identical stiffness and damping properties modeled by k_{T} and d_{T}.

Collecting the vertical accelerations of the train axle masses in $\ddot{\boldsymbol{q}}_{\mathrm{T,y}} \in \mathbb{R}^q$, the vertical train dynamics becomes

$$\boldsymbol{M}_{\mathrm{T}}\ddot{\boldsymbol{q}}_{\mathrm{T,y}} = -\boldsymbol{M}_{\mathrm{T}}\boldsymbol{g} + \boldsymbol{f}_{\mathrm{BT}} \tag{5}$$

where $\boldsymbol{M}_{\mathrm{T}} = \operatorname{diag}(m_{\mathrm{T},1}, \ldots, m_{\mathrm{T},q})$ and $\boldsymbol{g} = g\boldsymbol{e}$, $g = 9.81\mathrm{ms}^{-2}$, $\boldsymbol{e} = [1, \ldots, 1]^{\top} \in \mathbb{R}^q$. Given v_{T} and $\boldsymbol{t}_{\mathrm{T,x0}}$, the horizontal train axle positions, the contact points are given by

$$\boldsymbol{q}_{\mathrm{T,x}} = v_{\mathrm{T}}\left(t\boldsymbol{e} - \boldsymbol{t}_{\mathrm{T,x0}}\right). \tag{6}$$

C. Coupling of Train and Bridge Model

The forces $\boldsymbol{f}_{\mathrm{BT}} \in \mathbb{R}^q$ in (5) are the spring and damper forces acting on the train axle masses. These train axle forces depend on the relative vertical displacements and velocities of the train axle masses $\boldsymbol{q}_{\mathrm{T,y}}, \dot{\boldsymbol{q}}_{\mathrm{T,y}}$ and the bridge $\boldsymbol{q}_{\mathrm{BT,y}}, \dot{\boldsymbol{q}}_{\mathrm{BT,y}}$ at the contact points $\boldsymbol{q}_{\mathrm{T,x}}$

$$\boldsymbol{f}_{\mathrm{BT}} = -\boldsymbol{D}_{\mathrm{T}}\left(\dot{\boldsymbol{q}}_{\mathrm{T,y}} - \dot{\boldsymbol{q}}_{\mathrm{BT,y}}\right) - \boldsymbol{K}_{\mathrm{T}}\left(\boldsymbol{q}_{\mathrm{T,y}} - \boldsymbol{q}_{\mathrm{BT,y}}\right) \tag{7}$$

where $\boldsymbol{D}_{\mathrm{T}} = d_{\mathrm{T}}\boldsymbol{I}$ and $\boldsymbol{K}_{\mathrm{T}} = k_{\mathrm{T}}\boldsymbol{I}$. The contact points move along the bridge and if between the bridge nodes, $\boldsymbol{q}_{\mathrm{BT,y}}$ and $\dot{\boldsymbol{q}}_{\mathrm{BT,y}}$ are not contained in $\boldsymbol{q}_{\mathrm{B}}$ and $\dot{\boldsymbol{q}}_{\mathrm{B}}$ and must be interpolated

$$\boldsymbol{q}_{\mathrm{BT,y}} = \boldsymbol{N}\boldsymbol{q}_{\mathrm{B}} \text{ and } \dot{\boldsymbol{q}}_{\mathrm{BT,y}} = \boldsymbol{N}\dot{\boldsymbol{q}}_{\mathrm{B}} \tag{8}$$

where $\boldsymbol{N} \in \mathbb{R}^{q\times n}$ contains evaluations of the shape functions used for the FE-discretization. Details on the derivation and

structure of $\boldsymbol{N}$ can be found in [3] and [12]. The shape functions $\boldsymbol{N}$ are evaluated at the contact points $\boldsymbol{q}_{\mathrm{T,x}}$. Using (6), $\boldsymbol{N}(\boldsymbol{q}_{\mathrm{T,x}}) = \boldsymbol{N}(v_{\mathrm{T}}(t\boldsymbol{e} - \boldsymbol{t}_{\mathrm{T,x0}})) = \boldsymbol{N}(t)$, this is a function of time. To emphasize on this, the time dependency notation is kept in the following. Using (8), the train axle forces can be rewritten

$$\boldsymbol{f}_{\mathrm{BT}} = -\boldsymbol{D}_{\mathrm{T}}\left(\dot{\boldsymbol{q}}_{\mathrm{T,y}} - \boldsymbol{N}(t)\dot{\boldsymbol{q}}_{\mathrm{B}}\right) - \boldsymbol{K}_{\mathrm{T}}\left(\boldsymbol{q}_{\mathrm{T,y}} - \boldsymbol{N}(t)\boldsymbol{q}_{\mathrm{B}}\right). \tag{9}$$

The disturbance $\boldsymbol{z}_{\mathrm{B}}$ acting on the bridge model (II-A) is calculated from the train axle forces $\boldsymbol{f}_{\mathrm{BT}}$. When the contact points are between bridge nodes, $\boldsymbol{f}_{\mathrm{BT}}$ is distributed to the nearest bridge nodes using the shape functions $\boldsymbol{N}(t)$

$$\boldsymbol{z}_{\mathrm{B}} = -\boldsymbol{N}(t)^{\top}\boldsymbol{f}_{\mathrm{BT}}. \tag{10}$$

D. Full Bridge-Train Model

Substituting the disturbance (10) into the bridge model (II-A) and combining it with the train model (5) and the train axle forces (9), the complete coupled bridge-train model is

$$\ddot{\boldsymbol{\eta}}_{\mathrm{B},r} + \boldsymbol{D}_{\mathrm{B},r}\dot{\boldsymbol{\eta}}_{\mathrm{B},r} + \boldsymbol{K}_{\mathrm{B},r}\boldsymbol{\eta}_{\mathrm{B},r} = -\boldsymbol{\Phi}_{\mathrm{B},r}^{\top}\boldsymbol{N}(t)^{\top}\boldsymbol{f}_{\mathrm{BT}} + \boldsymbol{F}_{\mathrm{B},r}\boldsymbol{v}_{\mathrm{B}} \tag{11a}$$

$$\boldsymbol{M}_{\mathrm{T}}\ddot{\boldsymbol{q}}_{\mathrm{T,y}} = -\boldsymbol{M}_{\mathrm{T}}\boldsymbol{g} + \boldsymbol{f}_{\mathrm{BT}} \tag{11b}$$

$$\boldsymbol{f}_{\mathrm{BT}} = -\boldsymbol{D}_{\mathrm{T}}(\dot{\boldsymbol{q}}_{\mathrm{T,y}} - \boldsymbol{N}(t)\boldsymbol{\Phi}_{\mathrm{B},r}\dot{\boldsymbol{\eta}}_{\mathrm{B},r}) - \boldsymbol{K}_{\mathrm{T}}(\boldsymbol{q}_{\mathrm{T,y}} - \boldsymbol{N}(t)\boldsymbol{\Phi}_{\mathrm{B},r}\boldsymbol{\eta}_{\mathrm{B},r}) \tag{11c}$$

$$\boldsymbol{y}_k = \boldsymbol{C}_{\mathrm{B},r}\boldsymbol{\eta}_{\mathrm{B},r}(k\Delta t) + \boldsymbol{w}_k \tag{11d}$$

$$\boldsymbol{\eta}_{\mathrm{B},r}(0) = \boldsymbol{\Phi}_{\mathrm{B},r}\boldsymbol{q}_{\mathrm{B},0},\ \dot{\boldsymbol{\eta}}_{\mathrm{B},r}(0) = \boldsymbol{\Phi}_{\mathrm{B},r}\boldsymbol{q}_{\mathrm{B},1}$$

$$\boldsymbol{q}_{\mathrm{T,y}}(0) = \boldsymbol{q}_{\mathrm{T,y},0},\quad \dot{\boldsymbol{q}}_{\mathrm{T,y}}(0) = \dot{\boldsymbol{q}}_{\mathrm{T,y},0}. \tag{11e}$$

Due to the time-dependency of $\boldsymbol{N}(t)$, the simulation model (11) is classified as an LTV system.

The train is characterized by $m_{\mathrm{T},1}, \ldots, m_{\mathrm{T},q}$, d_{T}, k_{T}, $\boldsymbol{t}_{\mathrm{T,x0}}$, and v_{T}. Parameter values for simulations are taken from the Eurocode [15], which defines a standard train comprising a leading and trailing four-axle power car, two three-axle end coaches, and 18 two-axle intermediate coaches; see Fig. 1. In [15], each train axle has the identical mass of $\bar{m}_{\mathrm{T}} = 17.33\mathrm{t}$. To account for different loadings, we assume different train axle masses $m_{\mathrm{T},k}t \in \left[90\%\bar{m}_{\mathrm{T}}, 110\%\bar{m}_{\mathrm{T}}\right]$ following a uniform distribution. The stiffness is $k_{\mathrm{T}} = (0.72 \cdot 2\pi)^2 \cdot \bar{m}_{\mathrm{T}} = 354.65\ \mathrm{kN/m}$, such that the first eigenfrequency associated with the bouncing mode of the train axle is 0.72 Hz [16]. Damping is set to $d_{\mathrm{T}} = 0.05 \cdot \bar{m}_{\mathrm{T}} + 0.005 \cdot k_{\mathrm{T}}$. High-speed trains often operate slightly below the maximum speed (e.g., $74\ \mathrm{ms}^{-1}$ for an ICE4-train [17]), therefore $v_{\mathrm{T}} = 66\ \mathrm{ms}^{-1}$. The vector $\boldsymbol{t}_{\mathrm{T,x0}}$ is determined by the wheelbases and v_{T}. The wheelbases for the power cars, end coaches, and intermediate coaches are illustrated in Fig. 1 and more information can be found in [15].

As mentioned before, vehicle-driven resonance occurs, if the quotient of train speed and wheelbases coincides with bridge eigenfrequencies. Here, the largest recurring wheelbase is the length of the intermediate cars $l_{\mathrm{ic}} = 16\ \mathrm{m}$. The first bridge eigenfrequency is $f_{\mathrm{B},1} = 5.49\ \mathrm{Hz}$. The resulting critical speeds can be calculated by $\boldsymbol{v}_{\mathrm{T},j} = f_{\mathrm{B},1} \cdot l_{\mathrm{ic}}/j, j = \{1, 2, \ldots\}$, see [3], and are $\boldsymbol{v}_{\mathrm{T},1} = 87.88\ \mathrm{ms}^{-1}$ and $\boldsymbol{v}_{\mathrm{T},2} = 43.94\ \mathrm{ms}^{-1}$. Both are conceivable train speeds, indicating that there is a risk of bridge resonances being hit.

III. Bridge State Estimation

The bridge state $\boldsymbol{x}_{\mathrm{B}} = [\boldsymbol{q}_{\mathrm{B}}^{\top}, \dot{\boldsymbol{q}}_{\mathrm{B}}^{\top}]^{\top}$ shall be estimated during the train crossing. Since the disturbance $\boldsymbol{z}_{\mathrm{B}} = -\boldsymbol{N}(t)^{\top}\boldsymbol{f}_{\mathrm{BT}}$ resulting from the bridge-train interaction is the decisive influence factor for displacements and vibration, it has to be taken into account, as previously shown in [12]. The approach taken in [12] is summarized in the following. Five cases of bridge state estimation are compared, whereby the estimator (Kalman filter) gets no or full information about the disturbance or bases on disturbance models of different complexity.

A. Considered Disturbance Models

Typically, the order of reduction for the estimation model is set smaller than that of the simulation model. In this work, the bridge model (II-A) is reduced to order $r_{\mathrm{est}} = 7$ for estimation. To evaluate the estimation performance, the system is considered open-loop, thus $\boldsymbol{u}_{\mathrm{B}} = 0$. The following five cases are considered.

1) The estimation model is the bridge model (II-A) with $\boldsymbol{z}_{\mathrm{B},1} = \boldsymbol{0}$, so the estimator gets no information about the disturbance.
2) The estimation model is the bridge model (II-A) with $\boldsymbol{z}_{\mathrm{B},2} = -\boldsymbol{N}(t)^{\top}\boldsymbol{f}_{\mathrm{BT}}$ (the simulated disturbance), so the estimator gets full information about the disturbance.
3) The estimation model is the bridge-train model (11), so the estimator includes the mass-spring-damper train model as the disturbance model. In this case, the vertical displacements and velocities of the train axle masses are part of the state vector. The disturbance $\boldsymbol{z}_{\mathrm{B},3}$ is inferred from the bridge and train state estimates from (11c).
4) The disturbance model is reduced to only the train axle weights, hence $\boldsymbol{f}_{\mathrm{BT}} \approx \boldsymbol{M}_{\mathrm{T}}\boldsymbol{g}$. The train vibration, so the dynamic part of (11b), $\boldsymbol{M}_{\mathrm{T}}\ddot{\boldsymbol{q}}_{\mathrm{T,y}}$, is neglected. The disturbance is then $\boldsymbol{z}_{\mathrm{B},4} = -\boldsymbol{N}(t)^{\top}\boldsymbol{M}_{\mathrm{T}}\boldsymbol{g}$. Since the train axle masses are constant, the disturbance model is named the MPL model.
5) The disturbance model is further simplified: Instead of individual train axle masses, the average train axle mass is taken, hence $\boldsymbol{z}_{\mathrm{B},5} = -\boldsymbol{N}(t)^{\top}\boldsymbol{g}\bar{m}_{\mathrm{T}}$. This disturbance model is referred to by average mass (AM)-MPL model.

B. Results

As expected, the estimates are clearly better, when the full information about the disturbance is available (case 2) in comparison to no available information (case 1). The RMSE of the estimates of case 1 in relation to those of case 2 is $e_1 = 165$. When using the mass-spring-damper train model as the disturbance model (case 3), the rmse in relation to case 2 is $e_3 = 9.63$. Despite using an accurate disturbance model, the

train state is inaccurately estimated which leads to an error in the time-varying part of the train axle forces $\boldsymbol{f}_{\mathrm{BT}}$, degrading the overall estimation performance. Therefore, the disturbance model is reduced to the essential, which are here the train axle weights (case 4) and the estimates are indeed better, $e_4 = 1.40$. Assuming an average train axle mass (case 5) barely reduces the estimation performance, $e_5 = 1.43$.

IV. Bridge State and Average Train Axle Mass Estimation

Based on the findings in from Section III, an SDE is proposed based on the bridge model (II-A) and the AM-MPL disturbance model (Section III-A, case 5). The train parameters using the AM-MPL model are v_{T}, $\boldsymbol{t}_{\mathrm{T},x0}$ and the average train axle mass $\bar{m}_{\mathrm{T}}$, of which v_{T}, $\boldsymbol{t}_{\mathrm{T},x0}$ are assumed to be known but $\bar{m}_{\mathrm{T}}$ shall be estimated in addition to the bridge state.

A. Estimation Model

Combining the bridge model (II-A) with the AM-MPL model, i.e., $\boldsymbol{z}_{\mathrm{B}} = -\boldsymbol{N}(t)^{\top}\boldsymbol{g}\bar{m}_{\mathrm{T}}$, gives the estimation model

$$\ddot{\boldsymbol{\eta}}_{\mathrm{B},r} + \boldsymbol{D}_{\mathrm{B},r}\dot{\boldsymbol{\eta}}_{\mathrm{B},r} + \boldsymbol{K}_{\mathrm{B},r}\boldsymbol{\eta}_{\mathrm{B},r} = -\boldsymbol{\Phi}_{\mathrm{B},r}^{\top}\boldsymbol{N}(t)^{\top}\boldsymbol{g}\bar{m}_{\mathrm{T}} + \boldsymbol{F}_{\mathrm{B},r}\boldsymbol{v}_{\mathrm{B}} \tag{12a}$$

$$\boldsymbol{y}_k = \boldsymbol{C}_{rb}\boldsymbol{\eta}_{\mathrm{B}}(k\Delta t). \tag{12b}$$

To use this continuous-time model (12) for a discrete state estimation design, it is discretized and rewritten in state-space representation. Using $\boldsymbol{x} = [\boldsymbol{\eta}_{\mathrm{B},r}^{\top}, \dot{\boldsymbol{\eta}}_{\mathrm{B},r}^{\top}]^{\top}$ as the system state

$$\dot{\boldsymbol{x}} = \boldsymbol{A}\boldsymbol{x} + \boldsymbol{B}_{\mathrm{z}}(t)\bar{m}_{\mathrm{T}} + \boldsymbol{B}_{\mathrm{u}}\boldsymbol{v}_{\mathrm{B}} \tag{13a}$$

$$\boldsymbol{y}_k = \boldsymbol{C}_{rb}\boldsymbol{x}(k\Delta t) \text{ with}$$

$$\boldsymbol{A} = \begin{bmatrix} \boldsymbol{0} & \boldsymbol{I} \\ -\boldsymbol{K}_{\mathrm{B},r} & -\boldsymbol{D}_{\mathrm{B},r} \end{bmatrix},\ \boldsymbol{B}_{\mathrm{z}} = \begin{bmatrix} \boldsymbol{0} \\ -\boldsymbol{\Phi}_{\mathrm{B},r}^{\top}\boldsymbol{N}(t)^{\top}\boldsymbol{g} \end{bmatrix}$$

$$\boldsymbol{B}_{\mathrm{u}} = \begin{bmatrix} \boldsymbol{0} \\ \boldsymbol{F}_{\mathrm{B},r} \end{bmatrix}, \qquad \boldsymbol{C} = \begin{bmatrix} \boldsymbol{C}_{\mathrm{B},r} & \boldsymbol{0} \end{bmatrix}. \tag{13b}$$

Model (13) is discretized at time step k to be

$$\boldsymbol{x}_{k+1} = \boldsymbol{F}\boldsymbol{x}_k + \boldsymbol{G}_{\mathrm{z},k}\bar{m}_{\mathrm{T}} + \boldsymbol{G}_{\mathrm{u}}\boldsymbol{v}_{\mathrm{B},k} \tag{14a}$$

$$\boldsymbol{y}_k = \boldsymbol{C}\boldsymbol{x}_k, \text{ with} \tag{14b}$$

$$\boldsymbol{F} = e^{\boldsymbol{A}\Delta t}$$

$$\boldsymbol{G}_{\mathrm{z},k} = \boldsymbol{A}^{-1}(e^{\boldsymbol{A}\Delta t} - \boldsymbol{I})\boldsymbol{B}_{\mathrm{z}}(k\Delta t)$$

$$\boldsymbol{G}_{\mathrm{u}} = \boldsymbol{A}^{-1}(e^{\boldsymbol{A}\Delta t} - \boldsymbol{I})\boldsymbol{B}_{\mathrm{u}}.$$

With zero-order hold for $\bar{m}_{\mathrm{T}}$ and $\boldsymbol{v}_{\mathrm{B}}$, it holds $\boldsymbol{x}_k = \boldsymbol{x}(k\Delta t)$. To estimate $\bar{m}_{\mathrm{T}}$, the state of the discrete model (14) is augmented by $\bar{m}_{\mathrm{T}}$. Since this value is constant, its dynamics are $\bar{m}_{\mathrm{T},k+1} = \bar{m}_{\mathrm{T},k}$. The resulting augmented model serves as an estimation model and is as follows:

$$\begin{bmatrix} \boldsymbol{x}_{k+1} \\ \bar{m}_{\mathrm{T},k+1} \end{bmatrix} = \begin{bmatrix} \boldsymbol{F} & \boldsymbol{G}_{\mathrm{z},k} \\ \boldsymbol{0} & 1 \end{bmatrix} \begin{bmatrix} \boldsymbol{x}_k \\ \bar{m}_{\mathrm{T},k} \end{bmatrix} + \begin{bmatrix} \boldsymbol{G}_{\mathrm{u}} \\ 0 \end{bmatrix} \boldsymbol{v}_{\mathrm{B},k} \tag{15a}$$

$$\boldsymbol{y}_k = \begin{bmatrix} \boldsymbol{C} & 0 \end{bmatrix} \begin{bmatrix} \boldsymbol{x}_k \\ \bar{m}_{\mathrm{T},k} \end{bmatrix}. \tag{15b}$$

The augmentation does not alter the LTV system property.

B. Estimation Method

Given the discrete LTV system (15) and assuming additive uncorrelated Gaussian zero-mean process and output noise, a discrete Kalman filter (KF) is optimal in the sense of minimizing the estimation error variance (also, see [18] and [19] for details on the algorithm) and therefore used. Due to the augmented state, it is often referred to as an AKF. The KF's sampling rate Δt is taken from the simulation output. To improve numerical stability, it is common to scale states and inputs to a similar range. In this study, the mass state is scaled with a factor of 10^5, as its value in kg is expected to be a five digit number. The process and simulation output noise covariance matrices $\boldsymbol{Q}$ and $\boldsymbol{R}$, respectively, are for simplicity set as diagonal matrices. The entries of $\boldsymbol{R}$ are set to 10^{-5}, matching the variance of the simulated output noise. The absolute values of the bridge velocities are three orders of magnitude larger than those of the bridge displacements, therefore the entries of $\boldsymbol{Q}$ are set to 10^{-7} for $\boldsymbol{q}_{\mathrm{B}}$ and to 10^{-4} for $\dot{\boldsymbol{q}}_{\mathrm{B}}$. Following the same argument, the $\boldsymbol{Q}$-entry for the scaled $\bar{m}_{\mathrm{T}}$ is set to 10^{-5}. The filter is initialized with $\hat{\boldsymbol{x}}_0 = \boldsymbol{0}$ and $\hat{\bar{m}}_{\mathrm{T},0} = 0$. The estimate covariance matrix is initialized as the identity matrix.

Since $\hat{\boldsymbol{x}}_k$ contains the estimates of $\boldsymbol{\eta}_{\mathrm{B},r}$ and $\dot{\boldsymbol{\eta}}_{\mathrm{B},r}$, the bridge state estimates are computed via

$$\hat{\boldsymbol{x}}_{\mathrm{B},k} = \begin{bmatrix} \hat{\boldsymbol{q}}_{\mathrm{B}} \\ \hat{\dot{\boldsymbol{q}}}_{\mathrm{B}} \end{bmatrix} = \begin{bmatrix} \boldsymbol{\Phi}_{\mathrm{B},r} & \boldsymbol{0} \\ \boldsymbol{0} & \boldsymbol{\Phi}_{\mathrm{B},r} \end{bmatrix} \hat{\boldsymbol{x}}_k. \tag{16}$$

The estimates of the train axle forces $\boldsymbol{f}_{\mathrm{BT}}$ and the disturbance $\boldsymbol{z}_{\mathrm{B}}$ are inferred from $\hat{\bar{m}}_{\mathrm{T},k}$ by

$$\hat{\boldsymbol{f}}_{\mathrm{BT},k} = \boldsymbol{g}\hat{\bar{m}}_{\mathrm{T},k} \text{ and } \hat{\boldsymbol{z}}_{\mathrm{B},k} = -\boldsymbol{N}_k^{\top}\boldsymbol{g}\hat{\bar{m}}_{\mathrm{T},k}. \tag{17}$$

The proposed SDE is applied to the bridge-train model (11) with the parameters specified in Section II, in open loop with $\boldsymbol{v}_{\mathrm{B}} = \boldsymbol{0}$. At the simulation start, the train is 50 m before the bridge, enters the bridge at time t_{E}, leaves the bridge at time t_{L}, and the simulation ends some seconds after the train left the bridge. Fig. 2 compares the following values obtained from the simulated bridge-train model (11) and from the SDE: The y-displacement of the fourth bridge node (indicated by a blue dot in Fig. 1), the average train axle mass, the train axle force of the first train axle, and the disturbance acting on the fourth bridge node in y-direction. Before the train enters the bridge, the mass estimate remains at the initial condition $\hat{\bar{m}}_{\mathrm{T},0} = 0$. When the train enters the bridge, there is an almost immediate change close to the real value of $\bar{m}_{\mathrm{T}}$. The same behavior can be observed for the train axle force of the first train axle. For the disturbance acting on the fourth bridge node in y-direction, the error is too small to be appreciated in the plot. The rmses for all estimated disturbances $\boldsymbol{z}_{\mathrm{B}}$ from t_{E} onwards is $e(\hat{\boldsymbol{z}}_{\mathrm{B}}) = 0.0028$ MN. Despite neglecting the time-varying part of the train axle forces in the disturbance model of the estimator, the disturbance estimates match well the simulated values.

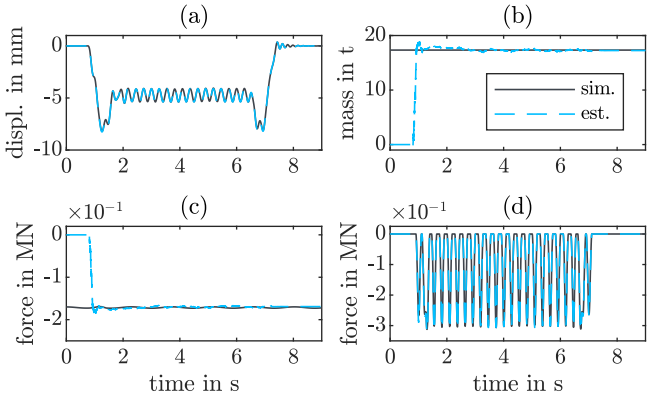

Fig. 2. Simulated versus estimated values for (a) the y-displacement of the fourth bridge node, (b) the average train axle mass, (c) the coupling force at the first axle, and (d) the disturbance acting in y-direction on the fourth bridge node.

C. Average Train Axle Mass Estimability Analysis

The Cramér–Rao bound (CRB) can be applied to evaluate the estimability of a model parameter $p \in \mathbb{R}$ and is applied to $\bar{m}_\mathrm{T}$ here. The CRB states that, under certain conditions ([20]), the variance of a parameter estimate $\hat{p}_k = \hat{p}(k\Delta t)$ any unbiased estimator can achieve is at least as large as the inverse FI evaluated for the real parameter p at $k\Delta t$

$$\mathrm{Var}[\hat{p}_k] \geq F_k(p)^{-1}. \tag{18}$$

Thus, the larger the FI, the smaller the CRB, the lower the bound on the variance, and thus the better estimates can be achieved ([20], [21]). The calculation of the FI is based on the following assumptions:

1) additive uncorrelated Gaussian zero-mean white noise on the output data, satisfied through the model assumptions in Section II;
2) constant real parameter p, satisfied since $p = \bar{m}_\mathrm{T}$.

Then, the output FI of p at $k\Delta t$ can be computed by

$$F_k(p) = \sum_{j=1}^{k} \frac{\partial \boldsymbol{y}}{\partial p}\bigg|_{j\Delta t}^{\top} \mathrm{Cov}[\boldsymbol{y}_j]^{-1} \frac{\partial \boldsymbol{y}}{\partial p}\bigg|_{j\Delta t} \tag{19}$$

where $\frac{\partial \boldsymbol{y}}{\partial p}\big|_{k\Delta t} := \boldsymbol{s}_{\mathrm{y},k} \in \mathbb{R}^p$ is the output sensitivity at $k\Delta t$. With $\boldsymbol{s}_\mathrm{x} = \frac{\partial \boldsymbol{x}}{\partial p}$ denoting the state sensitivity, for a system of the form $\dot{\boldsymbol{x}} = \boldsymbol{f}(\boldsymbol{x}, p)$, $\boldsymbol{y} = \boldsymbol{h}(\boldsymbol{x})$, the sensitivities $\boldsymbol{s}_\mathrm{x}$ and $\boldsymbol{s}_{\mathrm{y},k}$ can be computed via simulation of the sensitivity differential and output equation

$$\dot{\boldsymbol{s}}_\mathrm{x} = \frac{\partial \boldsymbol{f}}{\partial \boldsymbol{x}} \boldsymbol{s}_\mathrm{x} + \frac{\partial \boldsymbol{f}}{\partial p} \tag{20a}$$

$$\boldsymbol{s}_\mathrm{y} = \frac{\partial \boldsymbol{h}}{\partial \boldsymbol{x}} \boldsymbol{s}_\mathrm{x}, \ \boldsymbol{s}_\mathrm{x}(0) = \boldsymbol{0}, \quad t > 0. \tag{20b}$$

For model (13) with $p = \bar{m}_\mathrm{T}$ (20) are

$$\dot{\boldsymbol{s}}_\mathrm{x} = \boldsymbol{A}\boldsymbol{s}_\mathrm{x} + \boldsymbol{B}_\mathrm{z}(t) \tag{21a}$$

$$\boldsymbol{s}_{\mathrm{y},k} = \boldsymbol{C}\boldsymbol{s}_\mathrm{x}(k\Delta t). \tag{21b}$$

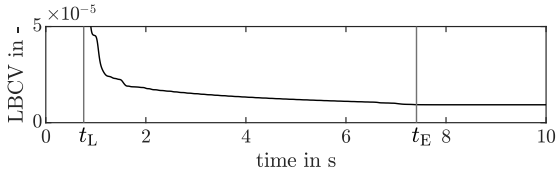

Fig. 3. LBCV for estimation of $\bar{m}_\mathrm{T}$ based on the AM-MPL model.

Since the simulation output noise has variance $\sigma_\mathrm{w}^2 = 10^{-5}$, the output covariance matrix in (19) is $\mathrm{Cov}[\boldsymbol{y}_j] = \sigma_\mathrm{w}^2 \boldsymbol{I}$, where $\boldsymbol{I}$ is the identity matrix. Using (21b) and (19), the CRB is computed as the inverse of the FI from (18). The estimate variance is normalized and denoted as the lower bound of the coefficient of variance (LBCV)

$$\mathrm{lbcv}_k(\bar{m}_\mathrm{T}) = \frac{1}{\bar{m}_\mathrm{T}} \sqrt{\frac{1}{F_k(\bar{m}_\mathrm{T})}}. \tag{22}$$

Fig. 3 shows the plot of the LBCV for the train axle mass $\bar{m}_\mathrm{T}$. The left and right vertical lines indicate the time t_E and t_L when the train enters and leaves the bridge, respectively. Before t_E, the train has no effect on the bridge motion, hence—as expected—the LBCV is infinite (i.e., $\bar{m}_\mathrm{T}$ cannot be estimated). For $t_\mathrm{E} < t < t_\mathrm{L}$, the LBCV decreases and the estimability of $\bar{m}_\mathrm{T}$ increases due to the growing amount of information. After t_L, no additional information on the train is gained and the LBCV remains constant.

D. Simulation Study Results

The performance of the proposed SDE is evaluated for the following parameters:

1) the number of cars (and thus $\boldsymbol{t}_{\mathrm{T,x0}}$, ref. Section III), thereby the number of power cars and end coaches is fixed, the number of intermediate coaches is varied;
2) $\bar{m}_\mathrm{T}$ (and thus k_T and d_T, ref. Section III);
3) v_T.

The parameter values are

$$\begin{aligned} \text{number of cars} &\in \{10, 16, 22\} \\ \bar{m}_\mathrm{T} &\in \{10, 15, 20\}\,\mathrm{t} \\ v_\mathrm{T} &\in \{35, 50, 65, 80\}\,\mathrm{m/s}. \end{aligned}$$

All possible combinations, for total of 36, are simulated. The results are evaluated and compared using five performance measures. The first measure is the LBCV after the train leaves the bridge, denoted by $\mathrm{lbcv}_\mathrm{end}$. The other four measures are the rmses of the estimates of the displacements and rotations $\hat{\boldsymbol{q}}_\mathrm{B}$ of the bridge nodes, the velocities $\hat{\dot{\boldsymbol{q}}}_\mathrm{B}$, the average train axle mass $\hat{\bar{m}}_\mathrm{T}$, and the disturbance $\hat{\boldsymbol{z}}_\mathrm{B}$. For each estimated value $\hat{\boldsymbol{\chi}}_k \in \mathbb{R}^{n_\chi}$ and the corresponding simulated value $\boldsymbol{\chi}_k \in \mathbb{R}^{n_\chi}$ at time step k, the rmse is defined as

$$e(\hat{\boldsymbol{\chi}}_k) = \sqrt{\frac{1}{N} \sum_{k=k_0}^{k_\mathrm{end}} \frac{1}{n_\chi} (\hat{\boldsymbol{\chi}}_k - \boldsymbol{\chi}_k)^\top (\hat{\boldsymbol{\chi}}_k - \boldsymbol{\chi}_k)}. \tag{23}$$

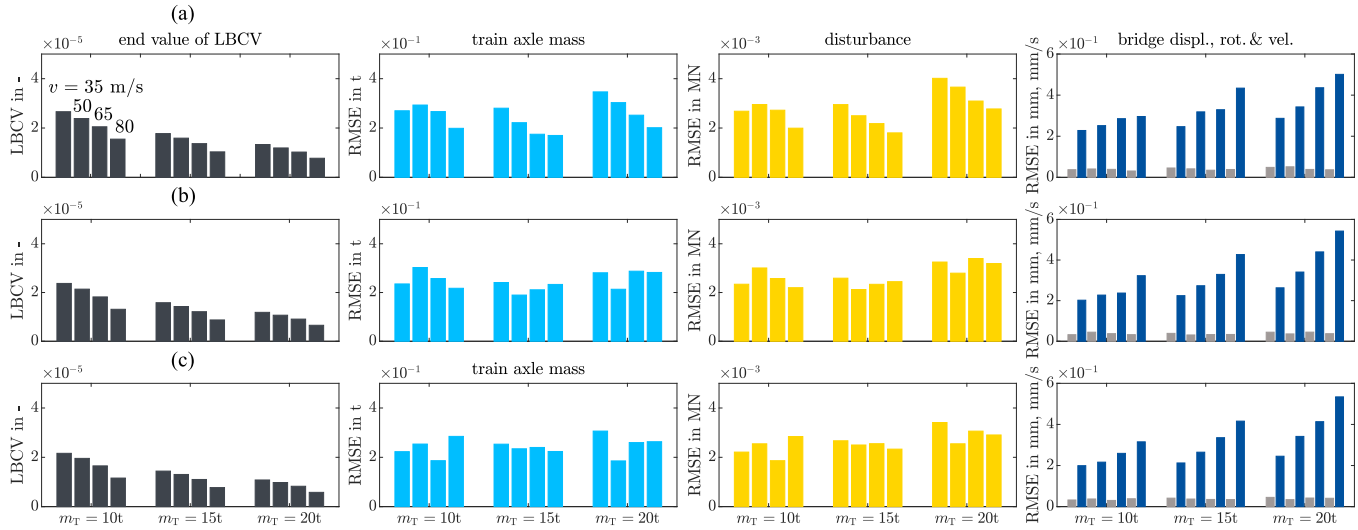

Fig. 4. Performance measures for the parameter study: LBCV (black); rmses of the estimates of the train axle mass (light blue), disturbance (yellow), bridge displacements and rotations (gray) with corresponding velocities (dark blue).

The rmses are computed for $t \in [t_E + 0.5\,\mathrm{s}, t_L + 0.05\,\mathrm{s}]$ with k_0 and k_{end} chosen accordingly and $N = k_{\mathrm{end}} - k_0 + 1$. The value of k_0 is chosen to leave out the error before the SDE converges after the train enters the bridge. If not taken into account, this would be a systematic, but unjustified corruption of the performance values.

Fig. 4 shows the bar charts of the performance metrics. Each row depicts results for one number of cars. Each column gives one of the performance measures: $\mathrm{lbcv}_{k_{\mathrm{end}}}$ in column 1, $e(\hat{\bar{m}}_T)$ in column 2, $e(\hat{\boldsymbol{z}}_B)$ in column 3, and $e(\hat{\boldsymbol{q}}_B)$ and $e(\hat{\dot{\boldsymbol{q}}}_B)$ in column 4. The results are grouped for each of the average train axle masses and each bar corresponds to a train speed. For all 36 cases, the time series are similar to those shown in Fig. 2. As the performance measures for all cases are each within the same order of magnitude (Fig. 4), the proposed SDE performs similarly for all parameter combinations.

A closer look reveals that for heavier and faster trains, a smaller $\mathrm{lbcv}_{k_{\mathrm{end}}}$ is calculated. Larger $\bar{m}_T$ and v_T cause a higher bridge excitation, which gives larger simulation output values and thus in this case more information available for estimation. However, for $e(\hat{\bar{m}}_T)$ no trend is visible, because when $\bar{m}_T$ and v_T increase, so does the train vibration, which is not included in the reduced disturbance model used in the SDE. For heavier trains, the train vibration is estimated into the train axle mass to a certain extent. This leads to larger oscillations of $\hat{\bar{m}}_T$, which in turn increase the rmse $e(\hat{\bar{m}}_T)$. Therefore, the modeling error due to the disturbance model reduction limits the quantitative estimability analysis, while qualitative results still fit.

Comparing the second and third column in Fig. 4, shows that the disturbance estimation error $e(\hat{\boldsymbol{z}}_B)$ is primarily related to the estimation error for the average train axle mass.

The values of $e(\hat{\boldsymbol{q}}_B)$ (gray, column 4) are similar for all parameter combinations while the values of $e(\hat{\dot{\boldsymbol{q}}}_B)$ increase for heavier and faster trains. Errors in $\hat{\boldsymbol{z}}_B$ mainly affect the amplitude of the oscillations of $\hat{\boldsymbol{q}}_B$ and $\hat{\dot{\boldsymbol{q}}}_B$. $\hat{\boldsymbol{q}}_B$ is composed of static displacements and oscillations during train crossing and has a large nonzero mean while the $\hat{\dot{\boldsymbol{q}}}_B$ oscillates with a near zero mean. So, errors in the amplitude of $\hat{\boldsymbol{q}}_B$ have a smaller impact on $e(\hat{\boldsymbol{q}}_B)$ than errors in the amplitude of $\hat{\dot{\boldsymbol{q}}}_B$ have on $e(\hat{\dot{\boldsymbol{q}}}_B)$.

V. Closed-Loop

The proposed SDE is evaluated in closed-loop in combination with an LQR for vibration damping. During the train crossing, the motion of the nodes of the bridge deck is composed of a slow downward displacement superimposed by high frequency oscillations; cf. Fig. 2(a). Because the compensation of the downward displacement can require high actuator forces, only the oscillations shall be damped. The control concept is based on [22]. In there, different model predictive control (MPC) schemes are compared, with and without input constraints for feasible actuator forces. The analysis carried out herein focuses on the applicability of an SDE within a feedback control loop. The input constraints are omitted such that the MPC-scheme reduces to an LQR.

A. Controller Design

The controller design bases upon the (nonaugmented) discrete AM-MPL model (14) and the disturbance is abbreviated as $\boldsymbol{z}_k = \boldsymbol{G}_{z,k}\bar{m}_T$. An operating point transition is performed using $\boldsymbol{x}_k = \Delta\boldsymbol{x}_k + \boldsymbol{x}_{s,k}$, $\boldsymbol{v}_{B,k} = \Delta\boldsymbol{v}_{B,k} + \boldsymbol{v}_{Bs,k}$, $\boldsymbol{z}_k = \Delta\boldsymbol{z}_k + \boldsymbol{z}_{s,k}$:

$$\overbrace{\Delta\boldsymbol{x}_{k+1} = \boldsymbol{F}\Delta\boldsymbol{x}_k + \boldsymbol{G}_u\Delta\boldsymbol{v}_{B,k} + \Delta\boldsymbol{z}_k}^{\Delta\text{-part}} \underbrace{-\boldsymbol{x}_{s,k+1} + \boldsymbol{F}\boldsymbol{x}_{s,k} + \boldsymbol{G}_u\boldsymbol{v}_{Bs,k} + \boldsymbol{z}_{s,k}}_{()_s\text{-part}}. \tag{24}$$

The Δ-part and the $()_s$-part of model (24) represent the oscillations and the quasistatic displacements, if the $()_s$-part is rendered zero as described in the following. First, the static part of the oscillating disturbance [cf. Fig. 2(d)] is approximated by taking

the average over the N_z time steps of the last period

$$\boldsymbol{z}_{\mathrm{s},k} = \frac{1}{N_\mathrm{z}} \sum_{j=1}^{N_\mathrm{z}} \boldsymbol{z}_{k-j+1}. \tag{25}$$

The period time T_z depends on v_T and the distances between the peak load causing wheel groups, here, in the area of the intermediate cars, $(16+2)\mathrm{m} = 18\mathrm{m}$. Thus, the period time is $T_\mathrm{z} = \frac{18\mathrm{m}}{v_\mathrm{T}}$ and hence $N_\mathrm{z} = \frac{T_\mathrm{z}}{\Delta t} = 273$. Second, since no static compensation is desired, $\boldsymbol{v}_{\mathrm{Bs},k} = \boldsymbol{0}$. Third, since $\boldsymbol{z}_{\mathrm{s},k}$ is chosen accordingly, $\boldsymbol{x}_{\mathrm{s},k}$ changes slowly in time and $\boldsymbol{x}_{\mathrm{s},k+1} = \boldsymbol{x}_{\mathrm{s},k}$ can be assumed. Using $\boldsymbol{z}_{\mathrm{s},k}$ and $\boldsymbol{v}_{\mathrm{Bs},k}$, the $()_\mathrm{s}$-part becomes zero if

$$\boldsymbol{x}_{\mathrm{s},k} = (\boldsymbol{I} - \boldsymbol{F})^{-1} \boldsymbol{z}_{\mathrm{s},k}. \tag{26}$$

An LQR is designed for the undisturbed Δ-part of model (24)

$$\Delta\boldsymbol{x}_{k+1} = \boldsymbol{F}\Delta\boldsymbol{x}_k + \boldsymbol{G}_\mathrm{u}\Delta\boldsymbol{v}_{\mathrm{B},k}. \tag{27}$$

The controller output is the solution to the optimization problem

$$\min_{\Delta\boldsymbol{v}_{\mathrm{B},k}} \sum_{k=0}^{\infty} \Delta\boldsymbol{x}_k^\top \boldsymbol{Q}_\mathrm{c} \Delta\boldsymbol{x}_k + \Delta\boldsymbol{v}_{\mathrm{B},k}^\top \boldsymbol{R}_\mathrm{c} \Delta\boldsymbol{v}_{\mathrm{B},k} \tag{28}$$

subject to the system dynamics (27). The solution of (28) depends mainly on the ratio of the weighting matrices $\boldsymbol{R}_\mathrm{c}$ and $\boldsymbol{Q}_\mathrm{c}$, therefore $\boldsymbol{R}_\mathrm{c} = \boldsymbol{I}$ is chosen. For $\boldsymbol{Q}_\mathrm{c}$, a diagonal weighting matrix for the full bridge state is chosen (entries belonging to the y-displacements and velocities of the bridge deck nodes are set to 10, the remaining entries are set to 0.001) and then transformed using (16). The solution of (28) is a linear state feedback controller

$$\Delta\boldsymbol{v}_\mathrm{B} = -\boldsymbol{K}_\mathrm{c}\Delta\boldsymbol{x}. \tag{29}$$

It holds $(\boldsymbol{F}, \boldsymbol{G}_\mathrm{u})$ is controllable and $(\boldsymbol{F}, \bar{\boldsymbol{Q}}_\mathrm{c})$, where $\boldsymbol{Q}_\mathrm{c} = \bar{\boldsymbol{Q}}_\mathrm{c}^\top \bar{\boldsymbol{Q}}_\mathrm{c}$, is observable. Thus (29) is a stabilizing controller for system (27) [23]. With $\boldsymbol{v}_{\mathrm{Bs},k} = \boldsymbol{0}$, the control input fed to the simulation model (11) is

$$\boldsymbol{v}_{\mathrm{B},k} = \Delta\boldsymbol{v}_{\mathrm{B},k} = -\boldsymbol{K}_\mathrm{c}\Delta\boldsymbol{x}_k = -\boldsymbol{K}_\mathrm{c}(\boldsymbol{x}_k - \boldsymbol{x}_{\mathrm{s},k}) \tag{30}$$

and $\boldsymbol{x}_{\mathrm{s},k}$ computed according to (26) and (25). When used with the proposed SDE, the controller relies on the estimated bridge state $\hat{\boldsymbol{x}}$ and average train axle mass $\hat{\bar{m}}_\mathrm{T}$. The estimation model (15) must be based on at least as many modes as those accounted for in controller model (27), thus $r_\mathrm{est} \geq r_\mathrm{ctrl}$. If the number of estimated modes is greater than the number of controlled modes, only the corresponding part of $\hat{\boldsymbol{x}}$ is used to compute the control input (30). In this work $r_\mathrm{ctrl} = r_\mathrm{est} = 7$.

B. Results

The following three cases are considered.

1) The dynamics of system (11) are simulated open-loop without controller.
2) The bridge state $\boldsymbol{x}$ and average train axle mass $\bar{m}_\mathrm{T}$ from the simulated dynamics of system (11) are used to compute the control input according to (30), (26), and (25).
3) The output of the SDE, the estimated bridge state $\hat{\boldsymbol{x}}$, and average train axle mass $\hat{\bar{m}}_\mathrm{T}$ are used in (30), (26), and (25).

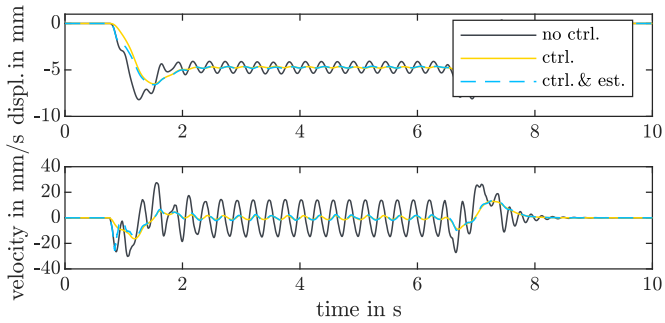

Fig. 5. Vertical displacement (a) and speed (b) of the fourth bridge node for the uncontrolled bridge (black), the controlled bridge with $\boldsymbol{x}$-feedback (yellow), and with $\hat{\boldsymbol{x}}$-feedback (blue).

Fig. 5 shows the y-displacement and -velocity of the fourth bridge node for the three cases. The control performance is measured using the rmse between the closed-loop (cases 2 and 3) and open-loop (case 1) y-displacements and -velocities of the bridge deck nodes. Using $\boldsymbol{x}$ and $\bar{m}_\mathrm{T}$ (case 2), the y-displacements and -velocities can be reduced by 60% and 53%, respectively. The performance reduces slightly when using the estimates $\hat{\boldsymbol{x}}$ and $\hat{\bar{m}}_\mathrm{T}$ (case 3) to 42% and 53%, for the y-displacements and -velocity, respectively. It can be concluded that the proposed SDE can effectively be used in closed-loop for vibration damping of the bridge under consideration.

VI. Conclusion

This article proposes an SDE for adaptive railway bridges: A bridge state and average train axle mass estimator based on a reduced disturbance model called AM-MPL model. For the estimator design, the bridge state is augmented by the average train axle mass and the simplicity of the reduced disturbance model causes the augmented model to be an LTV system allowing the use of an AKF. The estimability of the average train axle mass is analyzed via the CRB based on the FI. Simulation study results for different train parameter combinations indicate good estimability and accurate estimation of the bridge state and average train axle mass. Increasing the mass of the train leads to higher bridge excitation. This implies a larger modeling error between the mass-spring-damper train model used for simulation and the reduced disturbance model used in the SDE causing a slightly lower estimation accuracy. Finally, the estimator is evaluated in a closed-loop setup. An LQR is employed for damping oscillations around the static bridge deformation. The vibration amplitude is reduced by 60% when feeding back the simulated state and average train axle mass and by 53% when feeding back the estimates. Further research will investigate stochastic disturbances including rail roughness and rail-track deformations, a stability analysis of the full closed-loop and a validation using measurements of an existing railway bridge.

References

[1] P. Teuffel and W. Sobek, "Adaptive systems in architecture and structural engineering," *Smart Structures Mater.*, vol. 4330, pp. 36–45, 2001.

[2] F. Schlegl et al., "Integration of LCA in the Planning Phases of Adaptive Buildings," *Sustainability*, vol. 11, 2019, Art. no. 4299.
[3] A. P. Reksowardojo, G. Senatore, and L. Blandini, "Vibration control of simply supported beam bridges equipped with an underdeck adaptive tensioning system," in *Proc. IABSE Congr.*, Nanjing, 2022.
[4] G. Marzahn, "Requirements for the safety management of bridges in Europe: Results of the preliminary country query," in *Proc. Eur. Bridge Forum*, 2020, vol. 9.
[5] K. J. Keesman, *System Identification: An Introduction*, vol. 2. London, U.K.: Springer, 2011.
[6] W.-H. Chen, J. Yang, L. Guo, and S. Li, "Disturbance-observer-based control and related methods–An overview," *IEEE Trans. Ind. Electron.*, vol. 63, no. 2, pp. 1083–1095, Feb. 2016.
[7] E. Lourens, C. Papadimitriou, S. Gillijns, E. Reynders, G. De Roeck, and G. Lombaert, "Joint input-response estimation for structural systems based on reduced-order models and vibration data from a limited number of sensors," *Mech. Syst. Signal Process.*, vol. 29, pp. 310–327, 2012.
[8] K. Maes et al., "Verification of joint input-state estimation for force identification by means of in situ measurements on a footbridge," *Mech. Syst. Signal Process.*, vol. 75, pp. 245–260, 2016.
[9] E. Lourens, E. Reynders, G. De Roeck, G. Degrande, and G. Lombaert, "An augmented kalman filter for force identification in structural dynamics," *Mech. Syst. Signal Process.*, vol. 27, pp. 446–460, 2012.
[10] S. E. Azam, M. M. Didyk, D. Linzell, and A. Rageh, "Experimental validation and numerical investigation of virtual strain sensing methods for steel railway bridges," *J. Sound Vib.*, vol. 537, pp. 117–207, 2022.
[11] S. E. Azam, E. Chatzi, C. Papadimitriou, and A. Smyth, "Moving force identification: Optimal state estimation approach," *J. Sound Vib.*, vol. 239, pp. 233–254, 2001.
[12] A. Zeller et al., "State estimation using different disturbance models for adaptive railway bridges," in *Proc. IFAC World Congr.*, 2023.
[13] J. W. Strutt, 3. Baron Rayleigh, "The Theory of Sound," 1877.
[14] M. Böhm et al., "Input modeling for active structural elements-extending the established FE-Workflow for modeling of adaptive structures," in *Proc. IEEE Int. Conf. Adv. Int. Mech.*, 2020, pp. 1595–1600.
[15] EN Eurocode, "EN 1991-2 (2003) (English): Eurocode 1: Actions on structures - Part 2: Traffic loads on bridges," Authority: The European Union Per Regulation 305/2011, Directive 98/34/EC, Directive 2004/18/EC, 2003.
[16] T. Arvidsson, "Train–track-bridge interaction for the analysis of railway bridges and train running safety," Ph.D. dissertation, KTH Royal Institute of Technology, 2018.
[17] DB, "Der ICE 4: Das Rückgrat der DB-Fernverkehrsflotte," 2022. Accessed: May 30, 2023. [Online]. Available: http://www.deutschebahn.com/de/presse/sucheMedienpakete/medienpaketice4-6854650
[18] R. E. Kalman, "A new approach to linear filtering and prediction problems," *J. Basic Eng.*, vol. 82, no. 1, pp. 35–45, 1960.
[19] G. Welch and G. Bishop, "An introduction to the kalman filter," Tech. Rep. TR 95-041, 1995.
[20] A. van den Bos, *Parameter Estimation for Scientists and Engineers*. Hoboken, NJ, USA: Wiley, 2007.
[21] A. P. Schmidt, M. Bitzer, Á. W. Imre, and L. Guzzella, "Experiment-driven electrochemical modeling and systematic parameterization for a lithium-ion battery cell," *J. Power Sources*, vol. 195, pp. 5071–5080, 2010.
[22] S. Dakova et al., "A model predictive control strategy for adaptive railway bridges," in *Proc. IFAC World Congr.*, 2023.
[23] B. Molinari, "The stabilizing solution of the discrete algebraic Riccati equation," *IEEE Trans. Autom. Control*, vol. 20, no. 3, pp. 396–399, Jun. 1975.

Amelie Zeller received the M.Sc. degree in engineering cybernetics from the University of Stuttgart, Stuttgart, Germany, in 2021.

Since 2021, she has been a Research Assistant with the Institute for System Dynamics, University of Stuttgart. Her research interests include actuator placement and state and disturbance estimation for adaptive structures.

Spasena Dakova received the M.Sc. degree in engineering cybernetics, in 2019, from the University of Stuttgart, Stuttgart, Germany.

From 2018 to 2019, she was with the Systems Engineering Laboratory, Toyohashi University of Technology, Toyohashi, Japan. Since 2020, she has been a Research Assistant with the Institute for System Dynamics, University of Stuttgart. Her current research interests include modeling, analysis, and control design for adaptive structures.

Charlotte Stein received the M.Sc. degree in engineering cybernetics, in 2022, from the University of Stuttgart, Stuttgart, Germany.

Since spring 2022, she has been a Research Assistant with the Institute for System Dynamics, University of Stuttgart. Her research interests include state estimation of adaptive structures, data processing, and AI.

Michael Böhm received the Dipl.-Ing. and Ph.D. degrees in engineering cybernetics from the University of Stuttgart, Stuttgart, Germany, in 2011 and 2017, respectively.

Since 2017, he has been the Head of the Construction Systems Engineering Group with the Institute for System Dynamics, University of Stuttgart. His current research interests include dynamic modeling and control of mechanical and hydraulic systems, and distributed parameter systems with applications to civil engineering.

Gennaro Senatore is the Director of Research (Smart Structural Systems) with the Institute for Lightweight Structures and Conceptual Design (ILEK), University of Stuttgart, Stuttgart, Germany. He is also a Lead Expert for a preparatory action for the New European Bauhaus with the Joint Research Center (JRC) of the European Commission, Brussels, Belgium. He has Research Lead with the Swiss Federal Institute of Technology (EPFL), University College London, London, U.K., and London-based practice Expedition Engineering, London, U.K. His work uniquely combines structural optimization and control with computational design and sustainability to create high-performance and adaptive structural systems enabling new designs for civil and mechanical engineering.

Arka P. Reksowardojo received the M.Sc. degree, with a focus on indirect bridge frequency identification employing instrumented vehicles from the University of Tokyo, Tokyo, Japan, and the Ph.D. degree from the Swiss Federal Institute of Technology Lausanne (EPFL), Lausanne, Switzerland, in 2015 and 2020, respectively. In his doctoral thesis, he developed a design method for shape-morphing lightweight adaptive structures (https://youtu.be/x8kqWI07aSY).

He is a Postdoctoral Research Associate with the Institute for Lightweight Structures and Conceptual Design (ILEK), University of Stuttgart, Stuttgart, Germany. His current research interest includes the design of lightweight adaptive structures.

Lucio Blandini studied structural engineering at the University of Catania, Catania, Italy, and University of Bologna, Bologna, Italy, until 2000. He received the master's degree in architecture from the University of Pennsylvania, Philadelphia, PA, USA, and Architectural Association, London, U.K., in 2006, and the Ph.D. degree from the Institute for Lightweight Structures and Conceptual Design (ILEK), University of Stuttgart, Stuttgart, Germany, in 2005.

In this context, he developed and built the so-called Stuttgart Shell, a filigree glass-only shell structure spanning 8.5 m. After completing master's degree, a he took up a position as Project Manager with Werner Sobek. He has been partner as well as managing director since 2018. Since April 2020, he has also been the Head of ILEK and a Full-Time Professor with the University of Stuttgart. His most important projects include the Ferrari Museum in Modena, the special facades of the Japan Post Tower in Tokyo, the Etihad Museum in Dubai, the House of European History in Brussels, and Terminal 2 at Kuwait International Airport.

Oliver Sawodny (Senior Member) received the Dipl.-Ing. degree in electrical engineering from the University of Karlsruhe, Karlsruhe, Germany, 1991 and the Ph.D. degree in the field of model-based quality control from the Ulm University, Ulm, Germany, in 1996.

In 2002, he became a Full Professor with the Technical University of Ilmenau, Ilmenau, Germany. Since 2005, he has been the Director of the Institute for System Dynamics, University of Stuttgart, Stuttgart, Germany. His current research interests include methods of differential geometry, trajectory generation, and applications to mechatronic systems.

Cristina Tarín received the M.Sc. degree in electrical engineering from the Technical University of Valencia, Valencia, Spain, 1996 and the Ph.D. degree in Trajectory and Position Control of a Nonholonomic Autonomous Mobile Robot from the University of Ulm, Ulm, Germany, in 2001.

She has been teaching at the Universidad Carlos III of Madrid, Madrid, Spain, and was enrolled in several research labs with the Technical University of Valencia. Since 2009, she has been a Full Professor with the Department of System Dynamics, University of Stuttgart, Stuttgart, Germany. Her current research interests include signal processing and filtering as well as estimation and modeling.